NASA Technical Memorandum 110371

Reduction of Blade-Vortex Interaction (BVI) Noise through X-Force Control

Fredric H. Schmitz

September 1995

National Aeronautics and Space Administration

NASA Technical Memorandum 110371

Reduction of Blade-Vortex Interaction (BVI) Noise through X-Force Control

Fredric H. Schmitz, Ames Research Center, Moffett Field, California

September 1995

National Aeronautics and
Space Administration

Ames Research Center
Moffett Field, California 94035-1000

Nomenclature

$\overline{c_d}$ = average drag coefficient of the rotor

D_f = drag of the helicopter's fuselage and appendages, lb

f = equivalent flat plate drag area, ft^2

f_e = equivalent flat plate drag area of an aerodynamically generated X-force, ft^2

F_x = constant X-force, lb

g = gravitational acceleration, ft/s^2

H = H-force of the rotor, lb

k_1 = constant introduced to localize the induced velocity

m = mass of the helicopter, slugs

p = point on the disk where strong BVI occurs

R = rotor radius, ft

T = thrust of the helicopter, lb

v = rotor induced velocity, ft/s

$\bar{v}$ = non-dimensional induced velocity, v/V_r

V = velocity or airspeed, knots (or ft/s)

V_r = momentum theory hover induced velocity, ft/s

V_T = rotor tip speed, ft/s

$\bar{V}$ = non-dimensional velocity, V/V_r

$\frac{dV}{dt}$ = acceleration parallel to the flight path, ft/s^2

W = gross weight of the helicopter, lb

α_{TPP} = tip-path-plane angle, deg

γ = flight path angle, deg

$\frac{d\gamma}{dt}$ = acceleration perpendicular to the flight path, rad/s

$\Delta\gamma$ = equivalent change in flight path angle, deg

λ_{TPP} = rotor tip-path-plane inflow, ft/s

$\bar{\lambda}$ = non-dimensional inflow, λ/V_r

μ = advance ratio, V/V_r

σ = rotor solidity

Reduction of Blade-Vortex Interaction (BVI) Noise through X-Force Control

FREDRIC H. SCHMITZ

Ames Research Center

Summary

Momentum theory and the longitudinal force balance equations of a single rotor helicopter are used to develop simple expressions to describe tip-path-plane tilt and uniform inflow to the rotor. The uniform inflow is adjusted to represent the inflow at certain azimuthal locations where strong Blade-Vortex Interaction (BVI) is likely to occur. This theoretical model is then used to describe the flight conditions where BVI is likely to occur and to explore those flight variables that can be used to minimize BVI noise radiation. A new X-force control is introduced to help minimize BVI noise. Several methods of generating the X-force are presented that can be used to alter the inflow to the rotor and thus increase the likelihood of avoiding BVI during approaches to a landing.

Introduction

Rotorcraft Blade-Vortex-Interaction (BVI) noise has been studied extensively over the past twenty years (refs. 1–6). Many experimental programs have been performed to help isolate the important governing parameters of the BVI noise. Mathematical models of all levels of sophistication from simple heuristic arguments to detailed Computational Fluid Dynamics (CFD) simulations have been developed and used to estimate the noise radiation in the hope that the improved understanding derived from these models can then be used to help mitigate the external noise radiation problem. Some success has been achieved—but BVI still remains one of the most difficult problems of the rotorcraft Industry.

This paper addresses the physics of the BVI problem on very simple terms and relates these physics to the task of using flight path control to minimize BVI noise. Deceleration and acceleration are shown to have powerful effects on potential BVI noise radiation. In addition, an auxiliary control called "X-force" is introduced that can be employed to avoid rotorcraft approach conditions where BVI occurs. Finally, some simple methods of generating X-force are discussed for several types of rotorcraft.

Necessary Conditions for BVI Impulsive Noise

For a helicopter in forward flight, it is well known that BVI noise occurs when the tip vortices shed from rotor blades near the front of the rotor disk pass in close proximity to the same or different rotor blades at later times near the rear and sides of the rotor disk. This is depicted in figures 1 and 2 from the top and side views respectively for a two bladed helicopter at an advance ratio of about 0.17 (from ref. 7).

The view from above the rotor, in a reference frame that moves with the rotor hub at the same velocity, shows the geometrical complexity of the problem (fig. 1). Tip vortices shed at azimuthal positions from approximately 90 to 270 degrees are swept rearward by the forward translational velocity, V, of the rotor where they appear to be intersected by the same or the opposite rotor at azimuthal positions from 270 to 90 degrees. The shed vortices and the bound vorticity of each blade also influence the exact position of the tip vortex filaments with respect to the following blade in this planar view. These apparent intersections are labeled 1 through 7 for this particular helicopter. The sketch at an instant in time of these vortex patterns was calculated from a classical "free wake" computation and shows the general nature of BVI pattern. It is known from many experimental studies that BVI occurs on both the advancing and retreating sides of the rotor. It is also known that the intensity of BVI is a function of many factors including; the strength and structure of the shed tip vortex that is passing in close proximity to the blade, the distance from the vortex to the blade at the vortex's closest point of passage to the blade, the local geometry of the interaction, the velocity of the blade relative to the air when the interaction occurs, and the relative trace tip-Mach number of the interaction. To say the least, the problem is very complicated and has yet to yield to robust and accurate mathematical predictions or computational simulations.

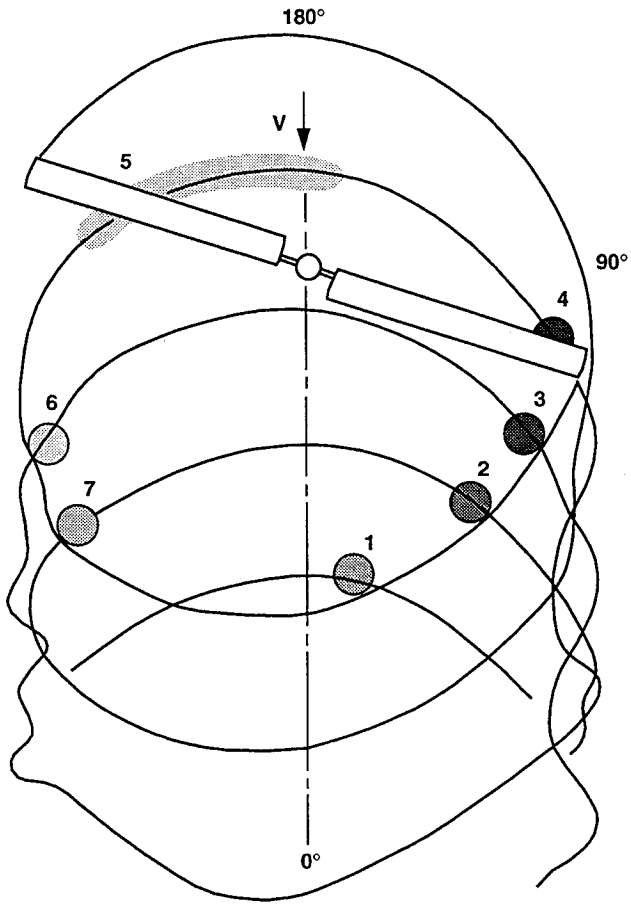

Figure 1. Top planar view of two bladed rotor tip-vortex pattern.

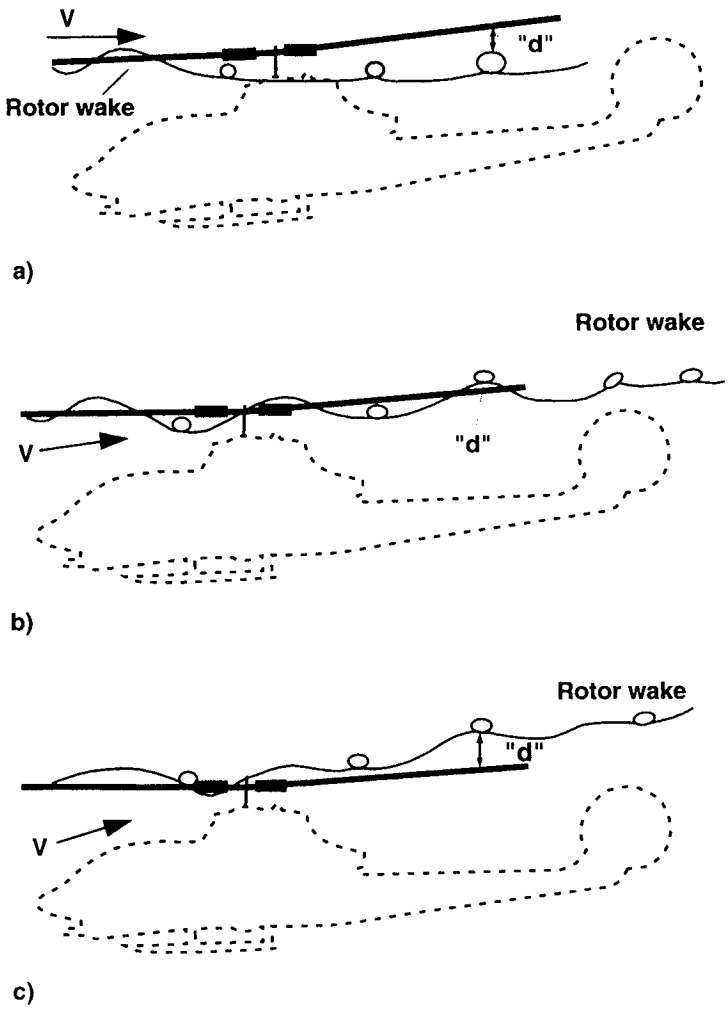

Figure 2. Side planar view of a single vortex filament for three descent conditions: (a) level flight, (b) normal descent, (c) steep descent.

The local geometry of the BVI interaction process is known to have a strong influence on BVI noise intensity and directivity. Near parallel interactions (interactions #2 and 3 in fig. 1) are known to radiate large amounts of acoustic energy. Interactions where the trace Mach number in space is near unity (interaction #4) are also suspected of radiating large amounts of acoustic energy. Unfortunately, patterns similar to those shown in figure 1 occur on all rotorcraft in non-axial flight. The only exception is in near hovering flight where the patterns are more circular in nature and do not lend themselves to either the near parallel nor trace Mach number 1.0 interactions.

Increasing the spacing between shed tip vortices and the interacting blades at the time of closest passage is a known method of reducing BVI noise. As depicted in figure 2 for a single tip vortex trajectory in the shed wake, the rotor wake system is first swept above the rotor but then is generally swept beneath the effective tip-path-plane of the rotor system in level steady-state flight (fig. 2(a)). At azimuthal positions where strong BVI occurs (when the vortex and the blade are nearly parallel), the shed tip vortex is an effective distance, "d," beneath the rotor tip-path-plane. Although "d" is depicted as a single value in figure 2, it is really a function of the particular interaction and the blade radius as each element of the blade comes closest to each passing tip vortex. It is known that all of the shed vortices move in the larger gross pattern as depicted in figure 2.

Changes in this effective distance cause strong changes in the resulting noise. As depicted in figure 2(b), normal descending flight changes the orientation of the forward velocity vector causing the shed tip vortices to pass closer to the tip-path-plane of the rotor. This strong BVI noise condition creates considerable noise and is typical of a landing approach for rotorcraft. At normal approach to landing speeds, the patterns shown in figures 1 and 2(b)

are typical for a two-bladed rotor system. Additional blades add to the complexity of the BVI problem by adding more potential interactions for the same advance ratio. Each time a blade passes in close proximity to a previously shed vortex, blade-vortex interaction noise is generated.

One known method of controlling this effective distance of the shed vortices from the following blades is through flight path control. As depicted in figure 2(c), further increases in rate of descent cause the majority of the vortices in the shed wake to pass above the tip-path-plane of the rotor. This increases the effective distance "d" and reduces the strength of the BVI noise radiation. This technique has been successfully used to help mitigate the noise on several helicopters (refs. 8 and 9).

Predicting the precise miss distance and the vortex characteristics during an encounter has not been possible with today's technology. The computer programs that have been developed to model the aerodynamics, structural dynamics, and wake of a non-axial rotor in near proximity to the fuselage do not capture the necessary detail. Consequently, accurate noise predictions are also not possible because they are directly related to the impulsive loading on each blade caused by these close vortex passages. Improved physical modeling and more accurate numerical representation of the wake system are required. However, while these codes have not always performed satisfactorily, they can be used to discern general trends for the BVI problem. First the codes must be adjusted to match experimental data by choosing key control factors (i.e., vortex core size, etc.). The codes are then exercised to predict trends. As long as the designs stay reasonably close to the fitted data-base, the results normally yield consistent trends.

A more simple, first-order approach, which is described below, is used in this paper to map out the regions where BVI is likely to happen. It is hypothesized that this simple approach is accurate enough to discern gross control and/or flight path strategies to avoid the likelihood of BVI noise.

First it is assumed that BVI noise is directly related to an average representative miss distance "d" for the most intense BVI encounters. These occur on the advancing side of the rotor disk when the blade is nearly parallel to the shed vortex (a "broadside" encounter) or when the time of travel from BVI encounter positions along the blade to an observer location is nearly constant. The larger "d's" depicted in figure 2 cause weaker BVI encounters and hence less noise while a "d" of near zero (head-on collision) causes large values of BVI noise radiation. The average miss distance can be calculated by using simple momentum theory and the balance of force equations for steady-state level flight to first estimate the average inflow through the rotor disk at chosen aggregate BVI azimuthal positions. The inflow can then be integrated to yield the average representative miss distance, "d." In practice, this last step is avoided and BVI is directly related to the net average inflow through the rotor disk. Little or no inflow through the rotor plane is postulated to cause high levels of BVI noise while large positive or negative inflow causes weak or negligible BVI noise.

Simplicity is the major advantage of using this approach. It yields good physical insight into the dominant (first-order) control and flight trajectory parameters that govern BVI noise and can easily be correlated with existing flight data. However, *this approach is not a precise calculation* and as such can not be used to discern quantitative changes in noise levels or for blade design. It also does not address the question of how the pilot flies the helicopter using real "pilot" controls to achieve the BVI noise reductions.

Tip-Path-Plane Angle and the Longitudinal Trim Equations

The longitudinal force balance equations for a typical single rotor helicopter depicted in figure 3 are shown below. The equations are written using a "wind axis system" which is typical in aircraft performance calculations. The wind axis system is chosen here for rotorcraft performance because it lends itself to simple physical interpretations. It should be noted that the wind axis system becomes ill defined (singular) in hovering flight—a performance state that is not considered in this paper.

X-Force Equation

$$T\sin(-\alpha_{TPP}) = D_f + W\sin\gamma + H\cos(-\alpha_{TPP}) + m\frac{dV}{dt} \quad (1)$$

Z-Force Equation

$$T\cos(-\alpha_{TPP}) = W\cos\gamma - H\sin(-\alpha_{TPP}) + mV\frac{d\gamma}{dt} \quad (2)$$

where

$$H = \frac{3}{8}\rho\sigma\pi R^2\mu V_T^2\overline{c_d} \quad \left(\text{or } H = \frac{3}{8}\rho\sigma\pi R^2 V V_T\overline{c_d}\right)$$

$$D_f = \frac{1}{2}\rho V^2 f$$

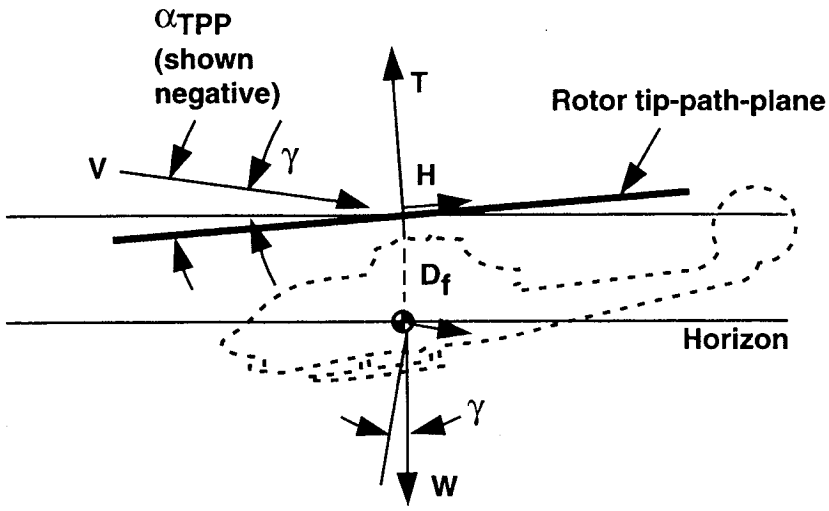

Figure 3. Longitudinal force balance (climbing flight).

For simplicity and ease of interpretation, assume that α_{TPP} and γ are small, then

$$\sin \alpha_{TPP} \approx \alpha_{TPP} \qquad \sin\gamma \approx \gamma$$

$$\cos \alpha_{TPP} \approx 1.0 \qquad \cos\gamma \approx 1.0$$

It is also known that the "H force" as resolved in the tip-path-plane is quite small at landing and takeoff airspeeds. For simplicity, it will also be neglected, i.e.,

$$H \approx 0$$

Equations 1 and 2 now become, to first-order

X-Force Equation

$$-T\alpha_{TPP} = D_f + W\gamma + m\frac{dV}{dt} \qquad (3)$$

Z-Force Equation

$$T = W + mV\frac{d\gamma}{dt} \qquad (4)$$

The term $mV\frac{d\gamma}{dt}$ represents the apparent force that occurs during "pull-ups" or "push-overs." During a flare prior to landing, it effectively requires the thrust to increase—to help arrest the helicopter's sink rate. During an approach to a landing the pilot normally tries to minimize large variations in flight path angle. Because small variations in $\frac{d\gamma}{dt}$ at landing approach speeds cause only small changes in thrust, changes in $\frac{d\gamma}{dt}$ will be neglected in this analysis.

Equation 4 now simply becomes T = W and can be substituted into equation 3, yielding:

X-Force Equation

$$\alpha_{TPP} = -\frac{D_f}{W} - \gamma - \frac{1}{g}\frac{dV}{dt} \qquad (5)$$

The tip-path-plane angle is simply governed by three terms: D_f, the fuselage drag (which also includes hub and interference drag); γ, the climb angle; and $\frac{dV}{dt}$, the acceleration parallel to the flight path.

Fuselage drag causes the tip-path-plane to become negative in trimmed flight. For an AH-1G helicopter with a 14 square foot equivalent drag area (f) at a nominal gross weight of 10,600 lb, the variation of D_f / W with velocity is shown in figure 4 by the curve labeled $\gamma = 0$. It can be seen that the tip-path-plane angle becomes more negative with increasing airspeed. The helicopter's main rotor must tilt forward to balance the drag in steady-state level flight.

Two scales are used in figure 4 to describe the helicopter's forward velocity. The non-dimensional scale depicted by $\bar{V}$ is defined to be the actual velocity, "V," divided by the momentum theory induced velocity in hover, V_r, where $V_r = \sqrt{\frac{W}{2\rho A}}$. For the AH-1G helicopter, $V_r = 38.9$ ft/s.

The effect of constant climb or descent angles is also illustrated in figure 4. Positive climb angles further decrease the tip-path-plane angle, while descents (negative γ) cause the tip-path-plane angle to become more positive. In non-accelerating flight, the climb angle can be chosen to maintain zero-tip-path plane angle (i.e., $\gamma = -D_f / W$).

Equation 5 also determines the effect of acceleration on the helicopter's tip-path-plane angle. Acceleration causes a decrease in α_{TPP} while deceleration causes an increase in α_{TPP}, an effect quite similar to the changes in climb angle. In fact, one could think of the effect of acceleration as a change in equivalent climb angle, i.e.,

$$\Delta\gamma_{Equivalent} \approx \frac{1}{g}\frac{dV}{dt} \qquad (6)$$

Thus, a 0.1g acceleration parallel to the flight path is equal to a change of 5.7 degrees of equivalent flight path angle and hence a change in tip-path-plane angle. Acceleration or deceleration parallel to the flight path has a strong influence on the helicopter's tip-path-plane angle (ref. 10).

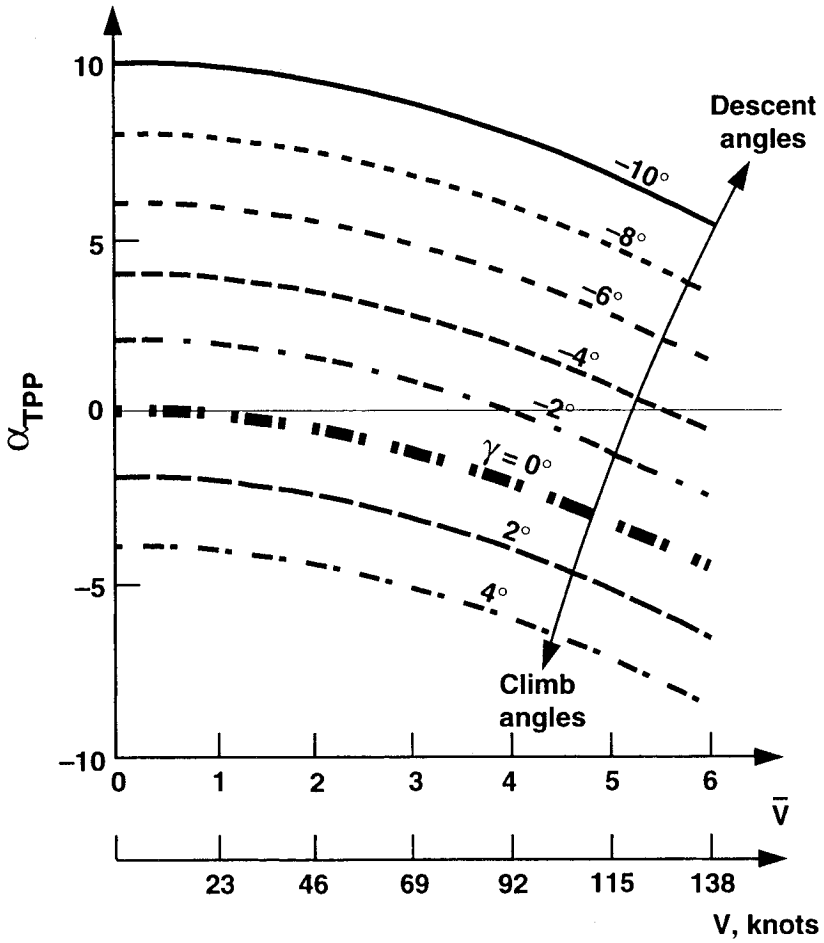

Figure 4. Tip-path-plane angle versus forward velocity for several climb and descent angles.

Some additional simplifying assumptions have been implicitly made in this balance of longitudinal force analysis that yields the explicit expression (eq. 5) for tip-path-plane angle. It has been assumed that the longitudinal pitching moment equation is satisfied and that the pitching moment controls employed (longitudinal cyclic, elevator angle, etc.) do not influence the balance of forces to first order. It has also been assumed that the engine supplies enough power to meet the required performance states. No real "pilot" controls have been introduced (collective, cyclic, etc.). Instead, it has been assumed that additional equations can be introduced along with their associated "pilot" controls that would determine the "pilot control" positions for each performance state.

This view of the rotorcraft performance problem is the classical one. The performance state of the rotocraft is determined by "X" and "Z" force balance equations. How to fly the aircraft to achieve this performance is determined after the outer loop performance is determined. In practice, some coupling of the moment and force balance equations does occur. In many cases the coupling is second order and can be neglected. The coupling has been neglected here to highlight the physics of the force balance equations.

The Effect of Flight path Control on Rotor Inflow

As discussed previously, the inflow through the rotor disk directly influences miss distances between the rotor blades and the shed tip vortices. This situation is diagramatically shown in figure 5. Rotor inflow normal to the tip-path-plane is defined to be

$$\lambda_{TPP} = V \sin \alpha_{TPP} - v \qquad (7)$$

where

$V \equiv$ velocity of the rotorcraft

$v \equiv$ induced velocity at any point on the rotor disk

Calculation of the inflow at any point on the rotor disk requires an accurate determination of rotor induced velocity. In general, the induced velocity is not uniform but varies markedly both fore and aft and laterally across the rotor disk. It is normally calculated using the strength of the vortex elements and the vortex element positions derived from a free-wake analysis and application of the Biot-Savart law.

A first order approximation to these miss distances can be obtained by using a variation of simple momentum theory and some knowledge of the non-uniform nature of the rotor's induced velocity. Because of the closeness of the rotor's wake to the tip-path-plane, it is assumed that the induced velocity field in the wake and in the rotor's tip-path-plane is the same. Initially, the induced velocity field is assumed to be constant across the rotor disk to be able to derive simple expressions relating the changes of induced velocity with changes in tip-path-plane angle. Then local variations in the induced velocity are accounted for and used in an approximate integration procedure to estimate the shortest distance of a point "p" in the rotor's wake from the rotor's tip-path-plane. In practice, the actual time integration is not formally carried out. The miss distance at point "p" is proportional to the local inflow through the rotor disk.

The classical momentum theory quartic relates the average induced velocity to the rotor's tip-path-plane angle and the forward velocity.

$$v^4 - 2Vv^3 \sin \alpha_{TPP} + V^2 v^2 + \left(\frac{T}{2\rho A}\right)^2 \qquad (8)$$

Because T = W, equations 7 and 8 can be non-dimensionalized by the hover induced velocity, $V_r = \sqrt{\frac{W}{2\rho A}}$. Remembering that α_{TPP} is assumed small, equation 7 becomes

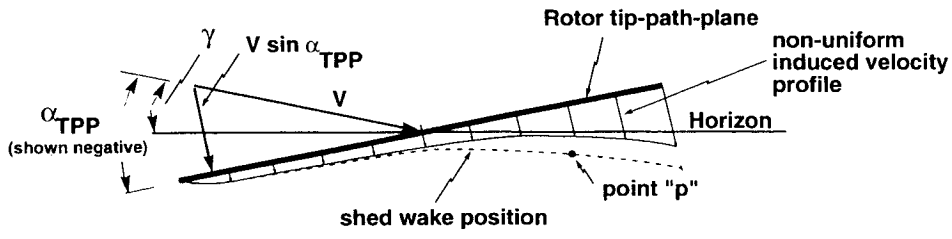

Figure 5. A two-dimensional sketch of the rotor's velocity field.

$$\bar{v}^4 - 2\bar{V}\bar{v}^3\alpha_{TPP} + \bar{V}^2\bar{v}^2 + 1 = 0 \qquad (9)$$

where

$$\bar{v} \equiv \frac{v}{V_r} \quad , \quad \bar{V} = \frac{V}{V_r}$$

This implicit equation can be solved for $\bar{v}$ by expanding the induced velocity in a first order Taylor series about small changes in α_{TPP}.

$$\bar{v} = \bar{v_o} + \frac{\partial \bar{v}}{\partial \alpha_{TPP}} \Delta\alpha_{TPP} + \text{higher order terms} \qquad (10)$$

The expressions $\frac{\partial \bar{v}}{\partial \alpha_{TPP}}$ and $\bar{v_o}$ are nonlinear functions of $\bar{V}$. Because uniform inflow and small angles are assumed, equation 7 becomes in non-dimensional form

$$\bar{\lambda}_{TPP} = \bar{V}\alpha_{TPP} - \bar{v} \qquad (11)$$

Substituting equation 10 into equation 11 yields

$$\bar{\lambda}_{TPP} = \bar{V}\alpha_{TPP} - \bar{v_o} - \frac{\partial \bar{v}}{\partial \alpha_{TPP}} \alpha_{TPP}$$

or

$$\bar{\lambda}_{TPP} = -\bar{v_o} + \left(1 - \frac{1}{\bar{V}} \frac{\partial \bar{v}}{\partial \alpha_{TPP}}\right)\bar{V}\alpha_{TPP} \qquad (12)$$

The final expression for uniform inflow is explicitly related to the rotor's tip-path-plane angle. The induced velocity for $\alpha_{TPP} = 0$ is plotted in figure 6. Induced velocity rapidly falls off as a function of non-dimensional forward velocity. The term $\left(1 - \frac{1}{\bar{V}} \frac{\partial \bar{v}}{\partial \alpha_{TPP}}\right)$ is plotted in figure 7. It represents the change in inflow with respect to a change in the flow normal to the rotor's tip path plane $\left(\bar{V}\alpha_{TPP}\right)$. In the limit as $\bar{V} \to 0$ (hover), it has a value of 0.5 but asymptotically approaches unity as $\bar{V}$ increases.

Equation 12 expresses uniform non-dimensional inflow though the rotor disk in terms of tip-path-plane angle and forward velocity. As discussed previously, it is known that the induced velocity across the rotor disk is not uniform. It is largest toward the rear of the disk and smallest or even negative over portions of the disk's advancing side in the second quadrant. The most intense blade-vortex interactions are known to occur on the advancing side of the disk in the first quadrant around $\psi \approx 45°$. The separation distances between the blade and the shed vortices at this azimuth position are directly affected by this less than uniform induced velocity field. To account for the non-uniformity in the induced velocity field, the factor K_1 is introduced which effectively reduces the inflow on the advancing side of the rotor disk where strong BVI is known to occur. In this analysis, 0.5 is nominally chosen. Equation 12 now becomes

$$\bar{\lambda}_{TPP} = -k_1\bar{v_o} + \left(1 - \frac{k_1}{\bar{V}} \frac{\partial \bar{v}}{\partial \alpha_{TPP}}\right)\bar{V}\alpha_{TPP} \qquad (13)$$

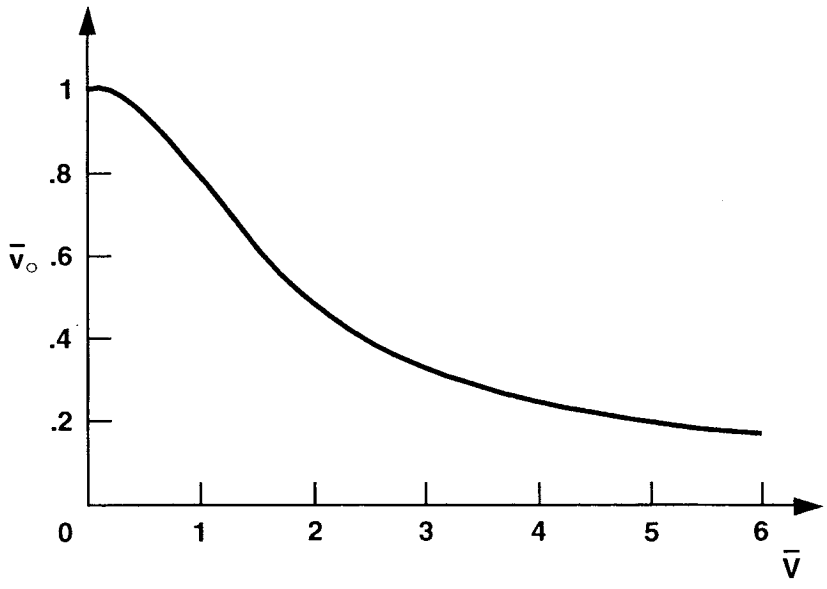

Figure 6. Non-dimensional induced velocity, $\bar{v_o}$, versus forward velocity, $\bar{V}$.

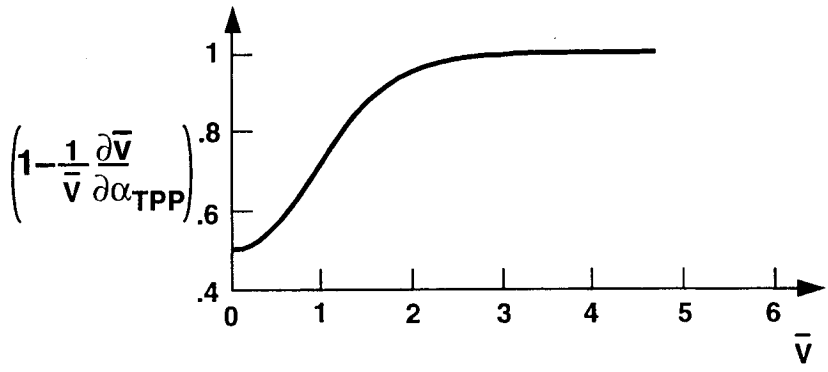

Figure 7. Inflow factor versus forward velocity.

If we define $k_2 = \left(1 - \frac{k_1}{\bar{V}} \frac{\partial \bar{v}}{\partial \alpha_{TPP}}\right)$ and substitute for α_{TPP} from the X-Force balance equation (eq. 5), we obtain

$$\bar{\lambda}_{TPP} = -k_1 \bar{v}_o - k_2 \bar{V}\left[\frac{D_f}{W} + \gamma + \frac{1}{g}\frac{dV}{dt}\right] \qquad (14)$$

This simple expression relates the estimate of the rotor inflow at a chosen point in the rotor disk to the drag of the helicopter, the helicopter's flight path angle, and the acceleration parallel to the flight path.

First, consider steady-state flight $\left(\frac{dV}{dt} = 0\right)$. Non-dimensional inflow is plotted as a function of non-dimensional forward velocity for chosen climb angles in figure 8. Fuselage drag and rotor induced velocity (when $\gamma = 0$) cause a negative inflow through the rotor system. Positive climb angles also add to the negative inflow through the rotor disk at all forward velocities. However, descents (negative climb angles) reverse this trend. As descent angle is increased, the inflow first becomes zero near a $\bar{V}$ of 4. This occurs at a descent angle of –4 degrees—a nominal approach descent angle for helicopter operations. As descent angle is increased further, the inflow through the disk changes sign and becomes positive. As indicated previously, near zero inflows are thought to be representative of BVI conditions. It also can be clearly seen that changes in climb angle make the largest changes in inflow at the higher forward velocities.

Changes in velocity (acceleration or deceleration) parallel to the flight path, which can be viewed according to equation 6 as an equivalent change in climb angle, have a similar effect on inflow through the rotor system. Accelerations are equivalent to positive climb angle changes and make the inflow through the disc more negative. Deceleration causes the disk to tilt aft and increase the positive inflow to the rotor.

These arguments can be used to explain why a helicopter on takeoff and/or in climbing flight very rarely exhibits BVI. Accelerations to higher velocities and positive climb angles both increase the negative inflow to the rotor system, which is already negative in level steady state flight. Near zero inflow conditions are not encountered and hence little or no BVI is generated.

However, the situation changes dramatically on approach to landings. Decelerations and descent angles both make the inflow more positive (rearward tilt of the rotor tip-path-plane). This positive inflow counteracts the negative inflow which is normal for level steady-state flight causing the net inflow through the rotor disk to become near zero—creating likely BVI conditions.

Pilots very rarely fly climb angles; rather they use rate of climb/sink gauges that are normally calibrated in ft/minute. Figure 9 replots non-dimensional inflow versus forward velocity as a function of rate of climb/sink. This simple model predicts near zero inflow conditions for a range of sink rates from about 550 ft/minute up to 1,000 ft/minute. To maintain zero inflow at lower non-dimensional forward velocities, larger sink rates are required to counteract the negative inflow arising from larger induced velocities typical at low airspeeds. At higher non-dimensional forward velocities, the larger sink rates again cause the inflow to become more positive, thus counteracting the negative inflow that results from the negative tip-path-plane angles that are required to balance larger values of drag. The zero inflow curve has an inflection point at non-dimensional velocities near 3.0. At this forward velocity, the smallest values of sink rate can cause nearly zero inflow conditions. Figure 9 also illustrates that rate-of-sink effectively controls inflow

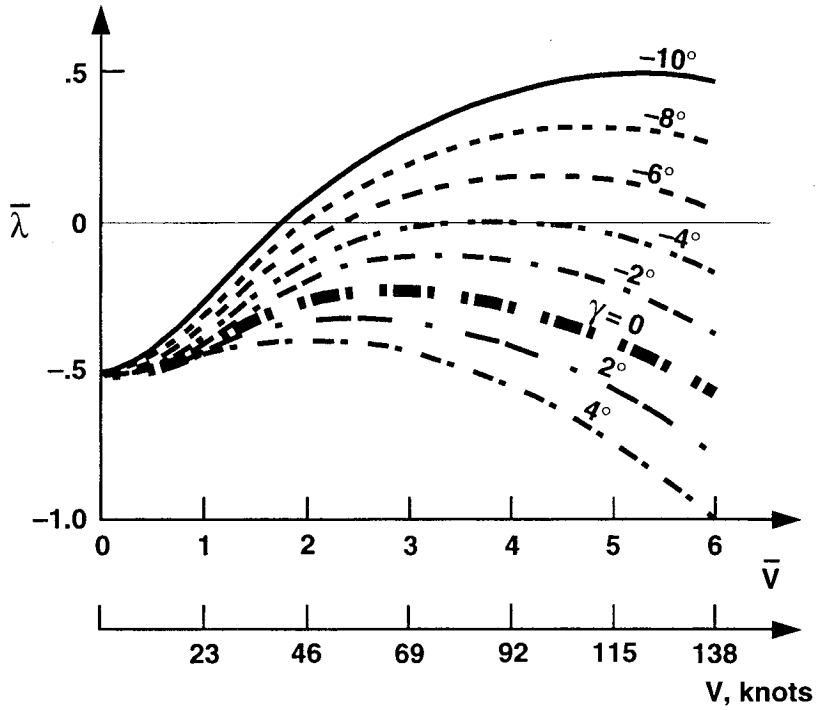

Figure 8. Non-dimensional Inflow at point "p" as a function of forward velocity for several flight path angles.

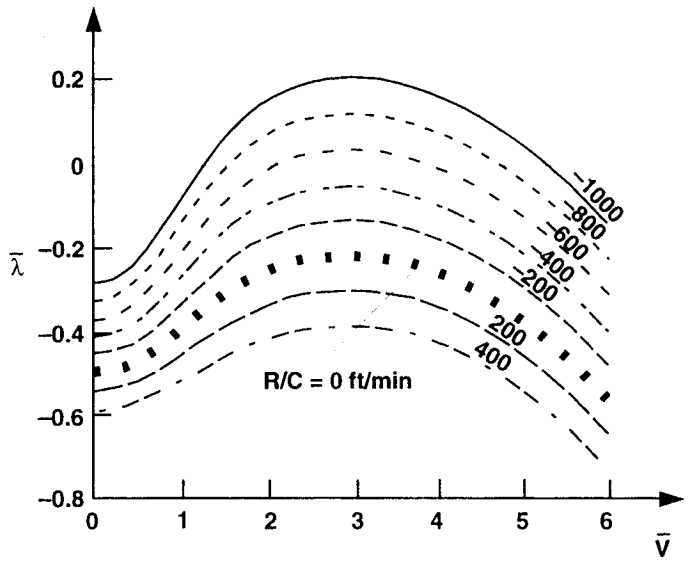

Figure 9. Non-dimensional inflow, $\bar{\lambda}$ versus forward velocity for several rates of climb.

over the entire forward velocity range; unlike climb/descent angle which was only really effective at high forward speeds.

The classical way of presenting regions where BVI noise is likely has been on a rate-of-sink versus forward velocity plot. (refs. 8 and 9). A replotting of equation 14 in this format for a series of non-dimensional inflows is shown in figure 10. Two scales are shown in this figure for velocity: a dimensional scale for the AH-1G helicopter and the non-dimensional scale used in the general analysis.

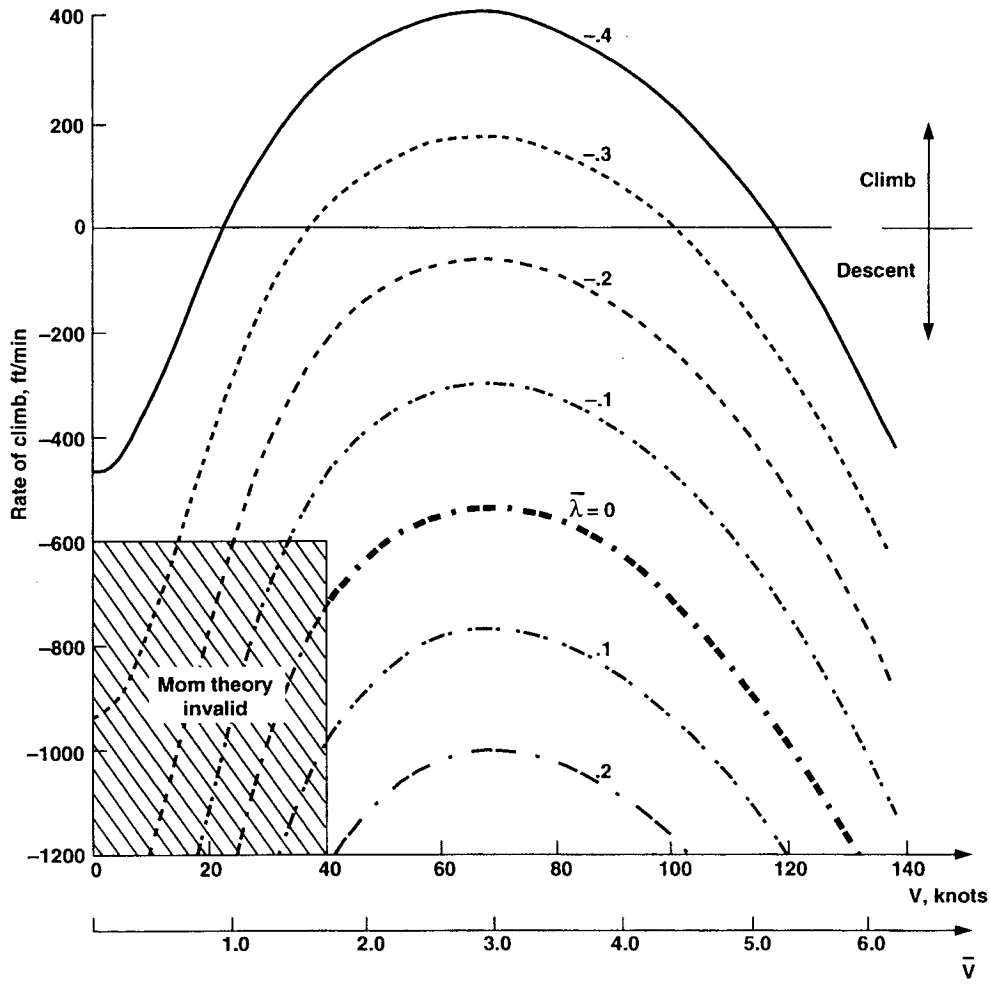

Figure 10. Rate of climb versus forward velocity for several values of non-dimensional inflow.

Inflow near zero is achieved at large sink rates at both low and high forward airspeeds according to figure 10. However, large sink-rates at low forward airspeeds are known to violate the assumptions of simple momentum theory. Therefore, at velocities below 40 knots at sink rates of less than 600 ft/minute, the simple theory presented here is invalid. This is not a serious problem for BVI noise predictions in most cases. Approach to landings are rarely done at airspeeds less than 40 knots. In addition, the epicycloid-like patterns of shed tip vortices are less likely to encounter following blades in near parallel interactions or have trace Mach numbers near unity at these slower airspeeds—conditions known to be necessary to generate strong BVI noise.

At velocities above 40 knots, the modeling predicts near zero inflow at approximately 550 ft/minute at 60–80 knots airspeeds. Above 80 knots, the sink rate to achieve zero net inflow through the rotor disk increases, becoming almost 1,000 ft/minute at 120 knots.

The HAI "Fly Neighborly Program" (ref. 9) uses similar knowledge of quiet regions in rate of sink versus forward space to help pilots minimize BVI noise. Based for the most part on noise measurements in the cabin of the helicopter, regions of loudest BVI noise levels were mapped out as shown in figure 11 for a medium weight helicopter (ref. 9). BVI for this 8,000 lb class helicopter is prevalent at about 400 ft/minute sink rate at about 60 to 80 knots—quite similar to the near zero inflow case predicted by this simple theoretical model.

The findings that the BVI region shown in figure 11 is closed and the theoretical curves shown in figure 10 do not yield closed regions needs some explanation. As discussed previously, this simple theory is invalid at airspeeds less than 40 knots at high sink rates. However, because BVI at these low airspeeds are not usually parallel encounters or do not have trace Mach numbers of 1, the radiated noise is not as intense as it is at higher

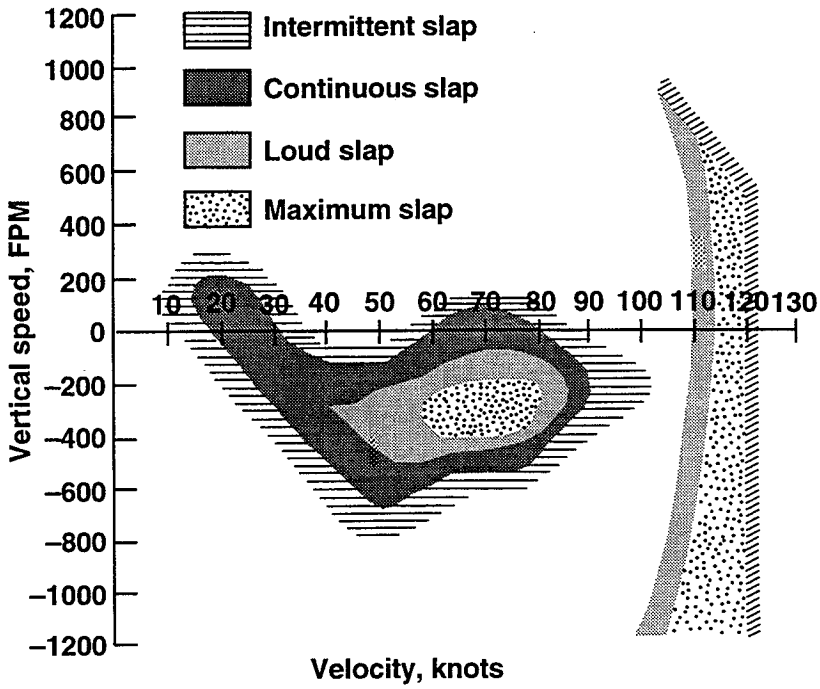

Figure 11. Measured cabin noise levels as a function of rate of climb and forward velocity, "fried egg plot" (from ref. 9).

airspeeds. The measured closed boundary at low airspeeds in figure 11 reinforces this hypothesis.

The measured BVI region in figure 11 also closes at higher airspeeds. This simple theory does not offer an explanation for this phenomenon either. In fact, the theory indicates that BVI will exist at higher airspeeds at higher sink rates. However, other measured full-scale acoustic data (refs. 11 and 12), taken in the acoustic far field using a flying microphone, support the theory. Strong BVI pulses were measured at high sink rates at high forward velocities. A possible explanation for these differences may be related to the fact that higher speed BVI noise may not always be able to be heard in the helicopter cabin. The strong BVI regions would appear to close as shown in figure 10, but in actuality helicopters flying under these conditions would still radiate BVI noise but in directions other than towards the helicopter cabin.

Additional acoustic data (ref. 13) from four approximately quarter scale model rotors also support the simple theory. A portion of the acoustic data for a "Boeing 360" model rotor test performed in the DNW wind tunnel is shown in figure 12 on a plot of shaft angle tilt versus advance ratio. The data were taken 25 degrees below the plane directly in front of the model rotor. Because the test was done using an isolated rotor in a wind tunnel, the inflow equation (eq. 14) has to be modified to reflect these conditions. There is no inflow due to climb, acceleration, or helicopter drag. In the wind tunnel for zero inflow, the rotor shaft must tilt aft to balance the negative inflow that arises from the rotor's induced velocity. The predicted zero inflow curve for the "Boeing 360" model rotor using this theory is superimposed on the data in figure 12. The trend of decreasing shaft tilt angle with increasing airspeeds is well predicted by the theory. This general trend is also confirmed in other model scale wind tunnel test programs (refs. 14 and 15).

A closer look at figure 12 and the other acoustic data of references 13–15 indicates that there are other factors that set the level of BVI noise. Within the general trend predicted by this momentum theory model, several small regions of larger intensity sometimes exist. The actual noise levels in these regions are dependent upon many design factors of the rotor itself as well as the acoustic phasing relationships of the BVI interactions. It also should be noted that model scale BVI data taken in wind tunnels have a tendency to under predict the measured full scale data (ref. 16) This is a possible explanation for a general lessening in the acoustic intensity levels with increasing airspeed at higher airspeeds in the model scale data of reference 12.

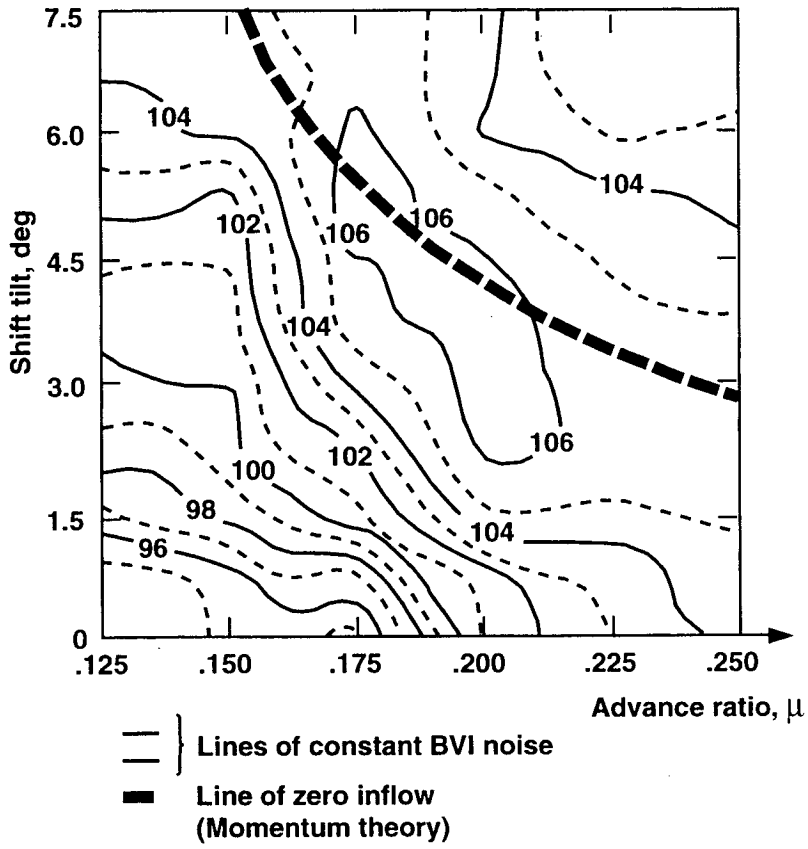

Figure 12. Noise level contours of the "Boeing 360" model rotor in the DNW tunnel as a function of shaft tilt (tip-path-plane angle) and advance ratio (from ref. 12).

Effect of X-Force Control

It has been shown through simple modeling that several flight parameters effectively control the inflow through the rotor disk and hence can influence the necessary conditions for BVI noise radiation. It then becomes natural to ask: Can the force balance be altered by introducing an additional control to change the occurrence of near zero inflow conditions?

The powerful nature of influencing inflow through X-forces has already been shown. Drag, rates of climb, and changes in velocity all directly control the tip-path-plane angle through the X-force balance, and hence control inflow through the rotor. As shown in equations 15 and 16 and depicted in figure 13, rewriting the force balance and inflow equations to include an "X-force" as a distinct independent control has a similar effect.

$$\alpha_{TPP} = \frac{-D_f}{W} - \gamma - \frac{1}{g}\frac{dV}{dt} - \frac{F_x}{W} \qquad (15)$$

$$\bar{\lambda}_{TPP} = -k_1\bar{v}_o - k_2\bar{V}\left[\frac{D_f}{W} + \gamma + \frac{1}{g}\frac{dV}{dt} + \frac{F_x}{W}\right] \qquad (16)$$

A positive X-force (fig. 13(b)) (a force in the drag direction) acts to further tilt the tip-path-plane forward (more negative α_{TPP}) and hence force the inflow through the rotor disk to be more negative. A negative X-force (fig. 13(c)), a propulsive force, causes the tip-path-plane to become more positive and makes the inflow become more positive until it passes upward through the rotor disk.

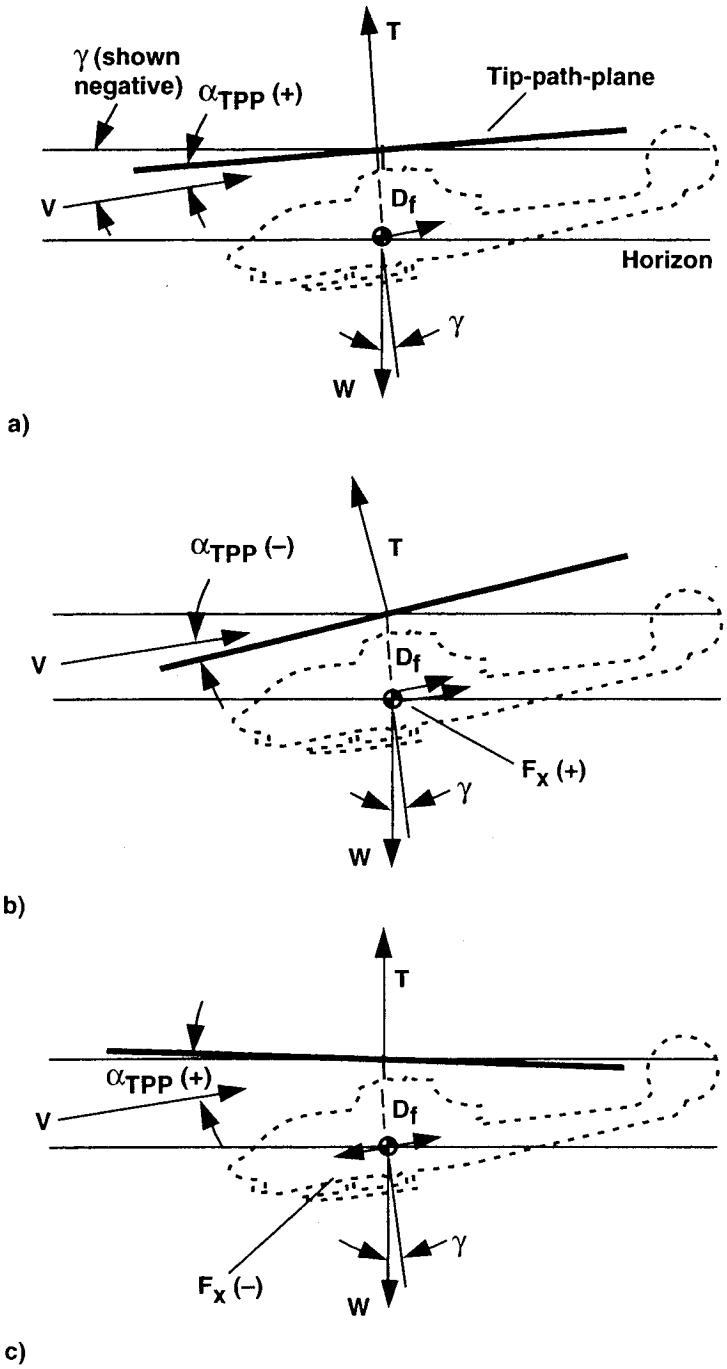

Figure 13. A schematic representation of the effect of X force control on the tip-path-plane angle (α_{TPP}) *in descending flight: (a)* $F_X = 0$*, (b)* F_X *positive, a drag force, (c)* F_X *negative, a propulsive force.*

The effect of a constant X-force which is independent of forward airspeed on the change in inflow through the rotor disk is shown by the solid curves in figure 14 for two levels of positive and negative $\frac{F_x}{W}$. Good tip-path-plane control and hence inflow control is shown for values of forward velocity above a $\bar{V}$ of 1.0. At high values of $\bar{V}$, X-force control becomes a powerful method of altering inflow and hence avoiding the likelihood of BVI noise radiation.

An X-force control that is proportional to velocity squared (a drag control device) is also plotted in figure 14 (dashed lines) as a function of forward velocity. Three levels of increased equivalent effective flat plate drag area are shown for the AH-1G helicopter: 14, 28, and 42 square feet. The change in inflow from this X-force drag control device is seen to be very effective at higher forward velocities but much less effective than a constant X-force control at lower velocities.

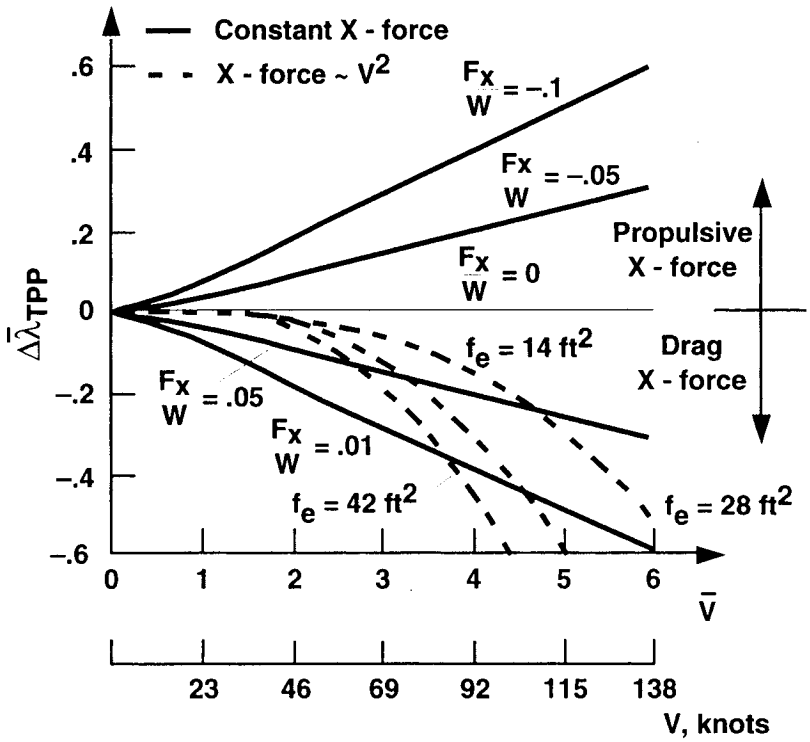

Figure 14. Change in inflow due to changes in X-force.

The effect that these two types of X-force control have on the predicted zero inflow curves is shown in figures 15 and 16. Above speeds of about 60 knots, both controls can be used to significantly alter the conditions where near zero inflow occurs. At or below 60 knots forward airspeed, drag control devices (fig. 16) lose their effectiveness and must be large to produce enough drag to significantly alter the inflow.

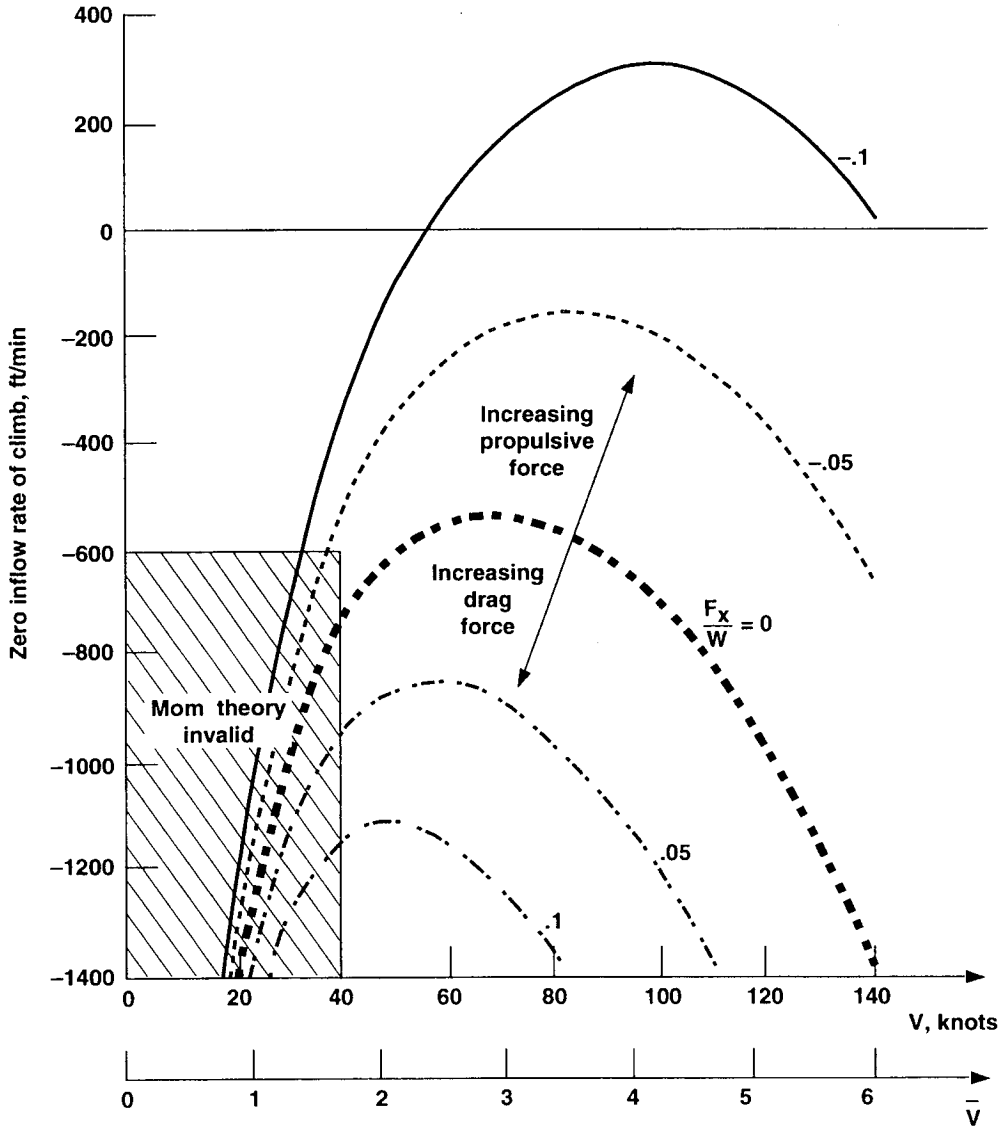

Figure 15. Rate of climb versus forward velocity curves for zero inflow with X-force = constant devices.

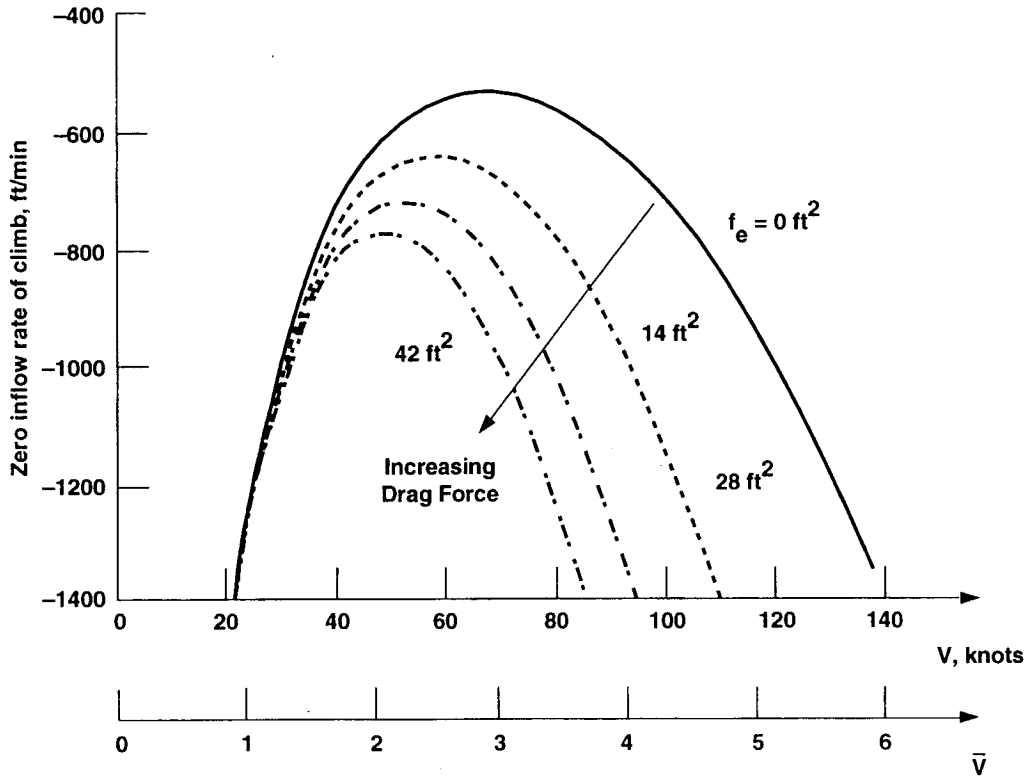

Figure 16. Rate of climb versus forward velocity curves for zero inflow with X-force aerodynamic drag devices $\left(F_x \sim V^2\right)$.

X-Force Controllers

A speed brake as sketched in figure 17 is one of the more simple X-force controllers. As hypothetically shown, panels can be mounted to the sides of the helicopter which, when employed, generate additional drag (X-force). In general, this class of devices will generate an X-force that is proportional to forward velocity squared and thus change the inflow according to the dashed curves in figure 14.

The effect of speed brake-like devices on the rate-of-sink versus forward velocity plots for a series of positive and negative inflows is shown in figure 18. An increase in the equivalent effective flat plate drag area of twice that of the AH-1G helicopter has been assumed to result from the deployment of these drag devices. When these curves are compared with the constant inflow curves of figure 10, significant changes are apparent. At a typical landing approach speed of 70 knots and 550 ft/minute rate-of-

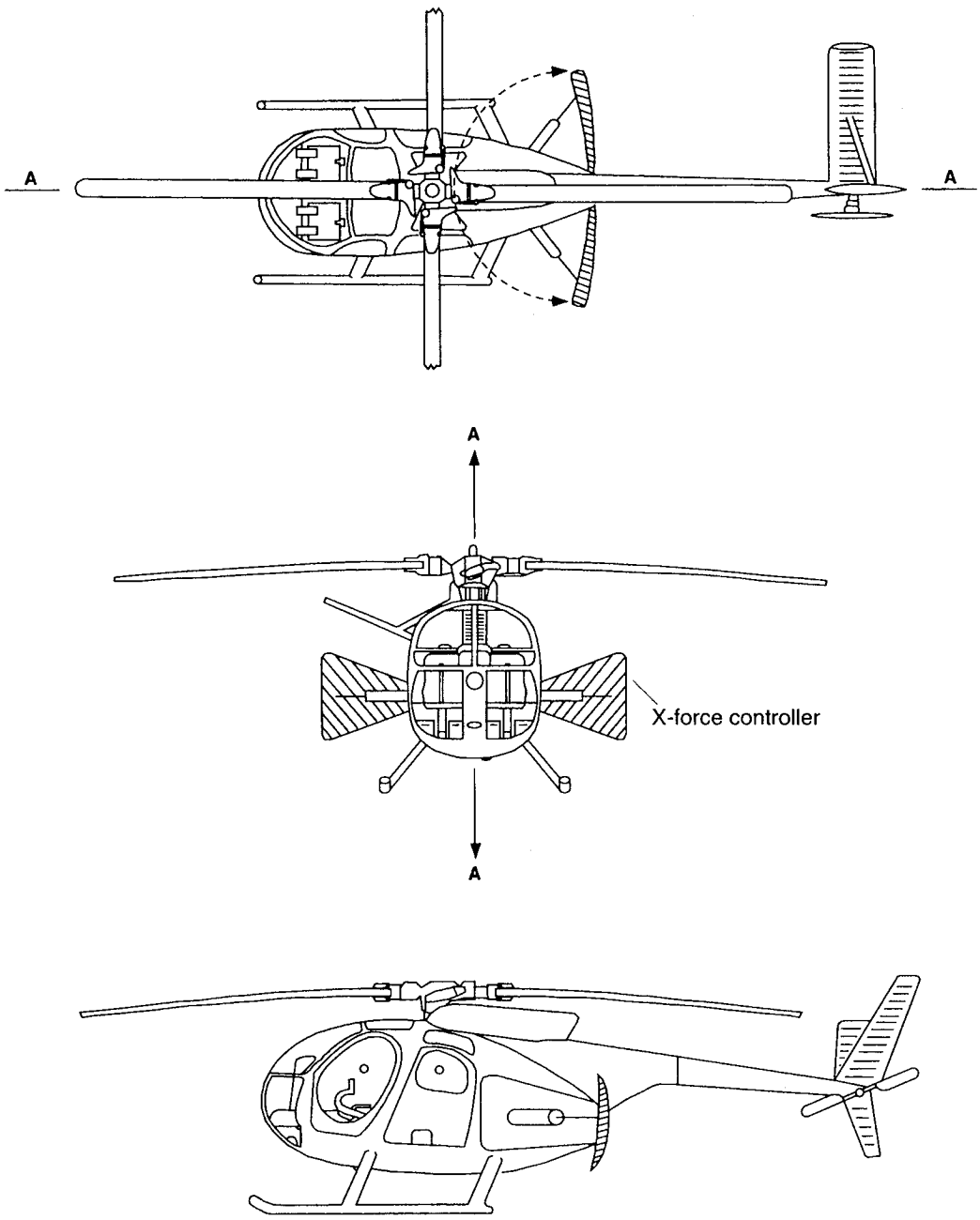

Figure 17. A sketch of an X-force "brake-like" device for a single rotor helicopter.

sink, the AH-1G was shown likely to produce significant amounts of BVI noise. Using the simple momentum theory model, near zero inflow was predicted to be likely. With the speed brake-like devices deployed, the zero inflow curve shifts downward—requiring higher sink-rates to produce the near zero inflow conditions. In effect, the tip-path-plane of the rotor has been forced to tilt-further forward to maintain X-force trim which increase the negative inflow through the rotor disk at the same sink rate. This increased inflow decreases the likelihood of strong BVI encounters at the 70 knots and 550 ft/minute landing approach conditions. As shown in figure 18, at 70 knots, it now takes about 850 ft/minute to generate the near-zero inflow condition and, as a consequence, produces the likelihood of strong BVI noise. At higher airspeeds, the effect on the flight profiles is even more dramatic.

Obtaining a pure aerodynamic X-force of significant magnitude from drag-like devices to alter the inflow through the rotor disk is an engineering challenge. Another potential method of generating the required

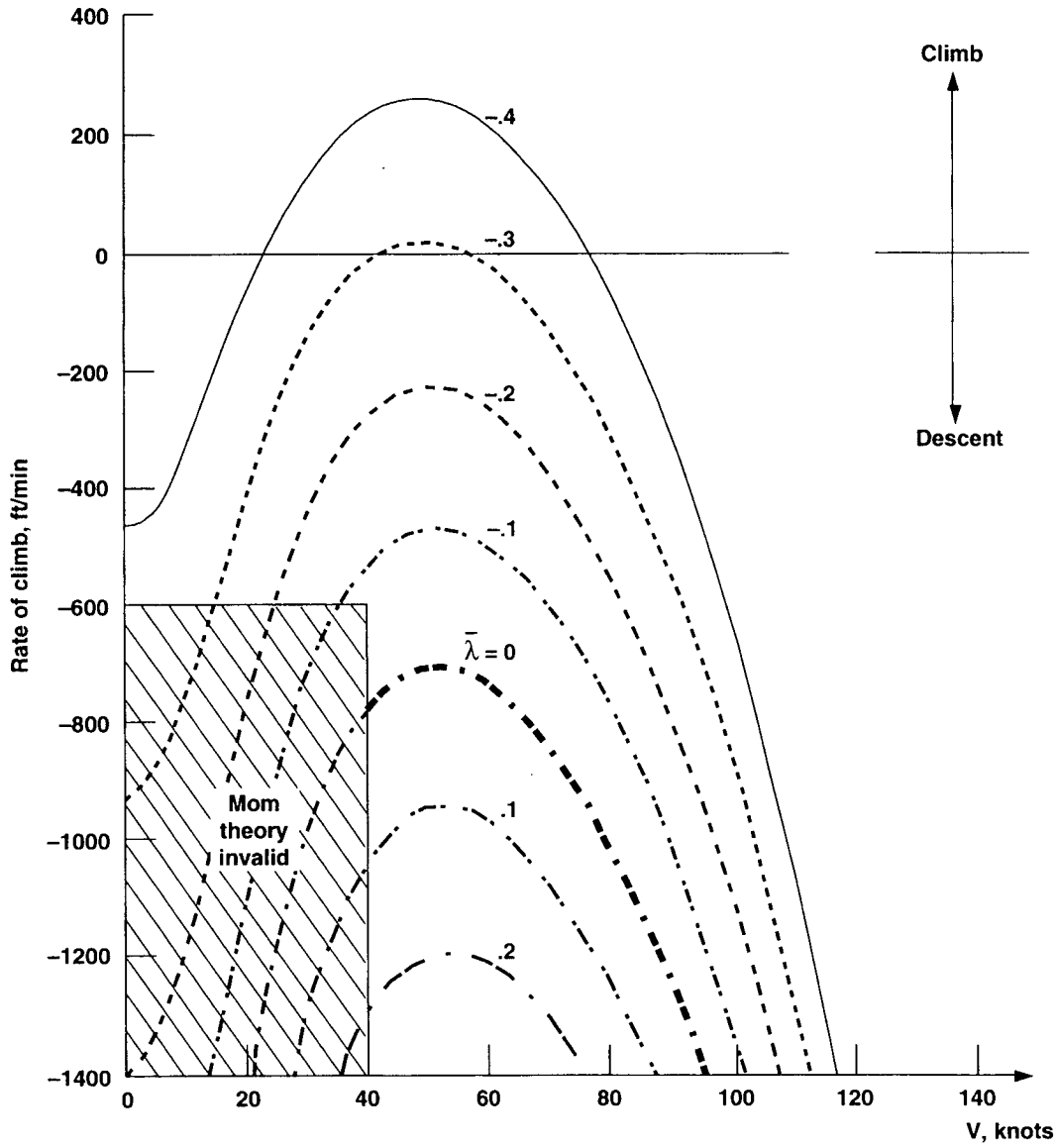

Figure 18. Rate of sink versus forward velocity for several values of inflow—aerodynamic drag devices deployed, $F_x \sim V^2$ *and* $f_e = 28\ ft^2$.

X-force is by employing a tilting wing (fig. 19). The wing is positioned in the near vertical position to reduce down-load near hover and to generate maximum drag during landing approach. At higher cruising airspeeds, the wing is rotated to carry lift. Generating sufficient X-force with this type of device is not thought to be a problem. There may also be an added benefit of having a wing to increase the high speed cruising capability of the helicopter.

There are obviously other engineering challenges associated with considering an aerodynamically generated X-force control to reduce BVI noise. The devices must be able to satisfy pitching moment constraints, be easily incorporated into piloting procedures, etc. However, the concept is conceptually not at all that revolutionary. Most airplanes prefer to carry some power on approach to a landing. Adding extra drag to a rotorcraft on approach will also require additional power for the same sink rates. In effect, the extra drag makes the helicopter fly in a more "takeoff-like" condition and thus reduce the likelihood of BVI noise.

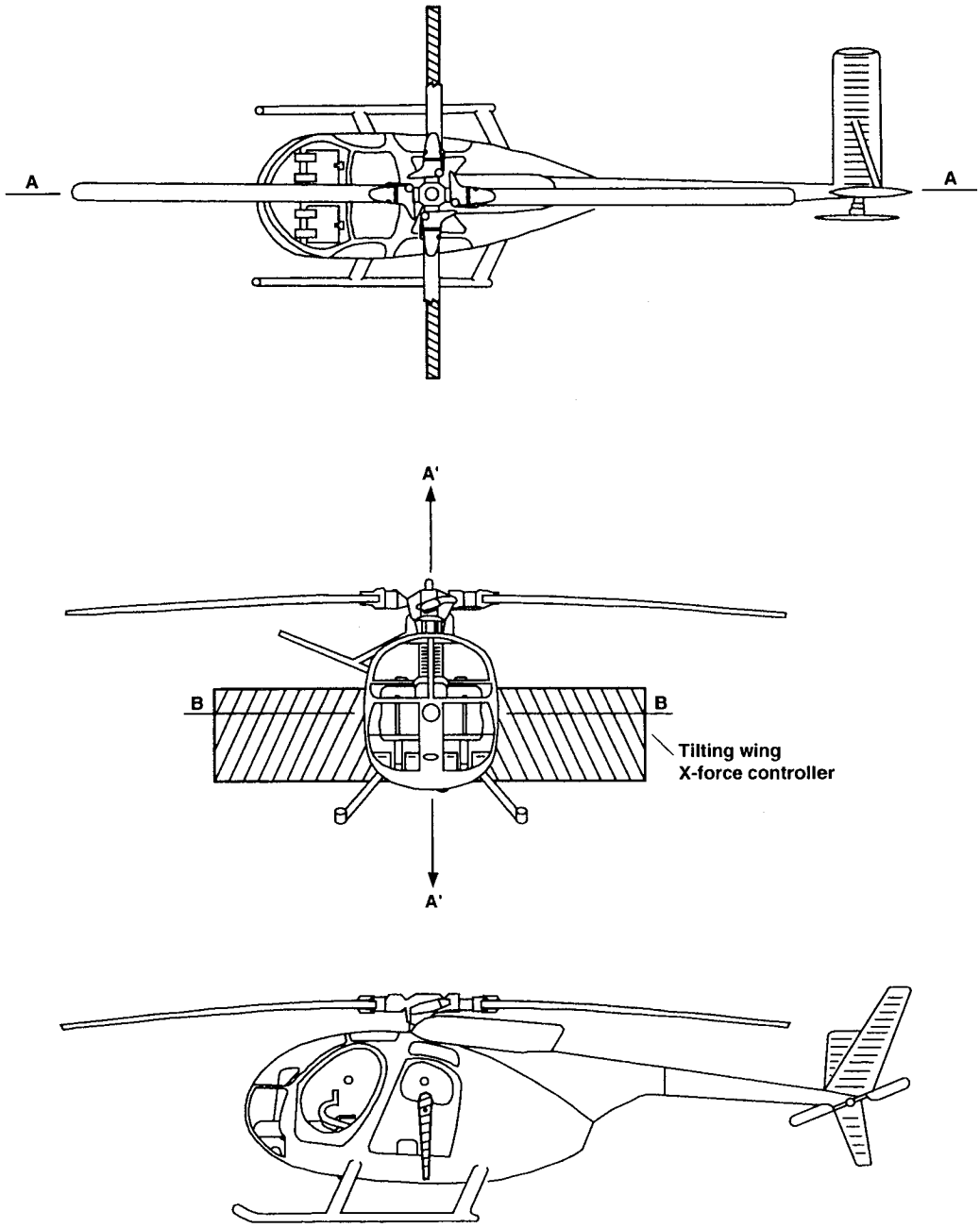

Figure 19. A sketch of a tilting-wing "brake-like" device.

A new concept of using X-force control to reduce BVI tilt-rotor noise is shown in figure 20. Large fold away drag-like panels are deployed along the wing to create aerodynamic drag (X-force) in landing approach conditions. The tip-path-plane angle of the tilting rotors is adjusted forward to account for the added effective drag of the X-force, creating additional negative inflow to the rotors. This additional negative inflow reduces the likelihood of BVI noise. In addition, these tilt-rotor drag devices might have the potential added benefit of reducing tilt-rotor download in near hovering flight.

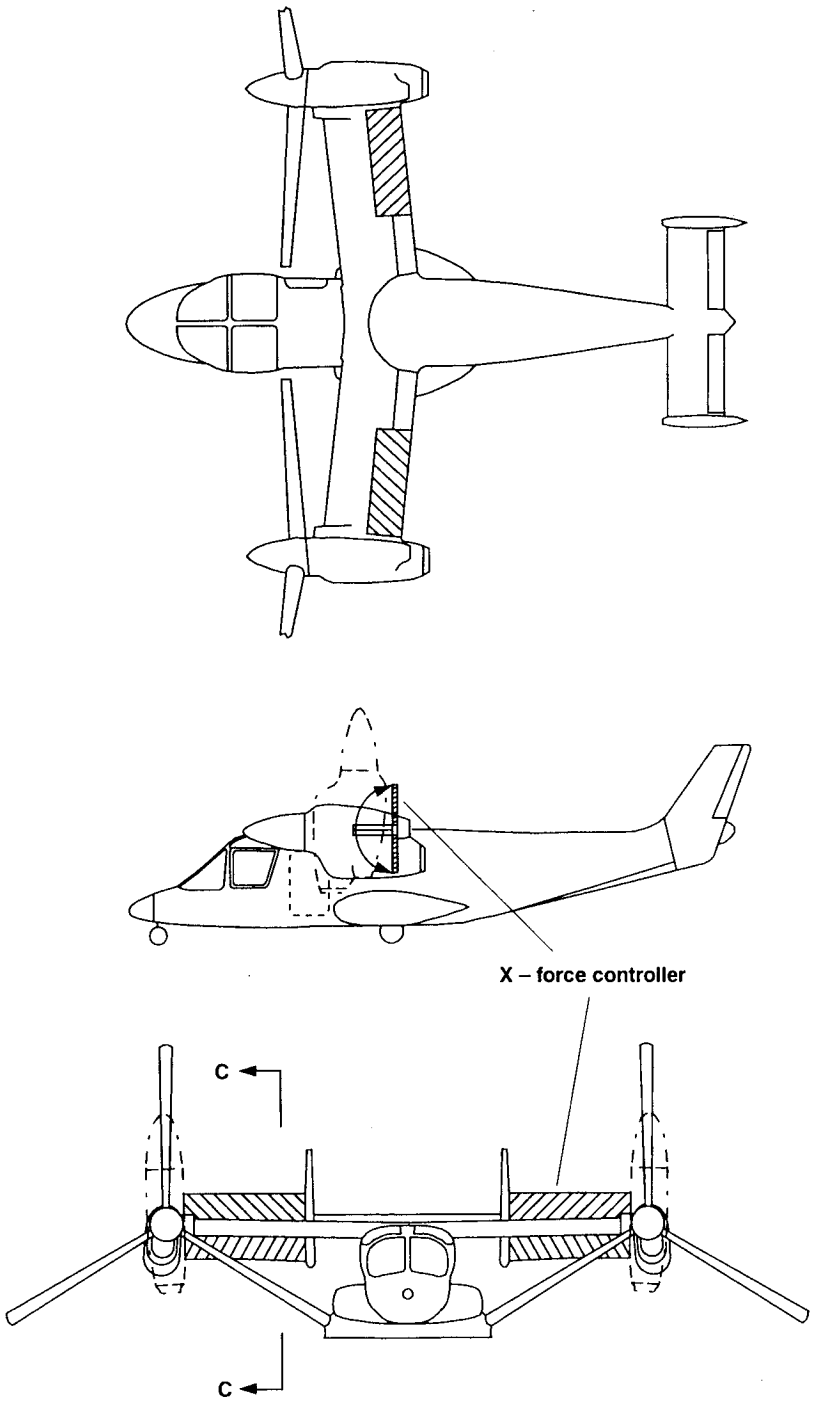

Figure 20. A possible aerodynamic X-force controller for tilt-rotor aircraft.

A sketch of a hypothetical constant X-force controller is shown in figure 21. In this case, two ducted propellers are mounted to either side of the fuselage to produce an effective X-force (drag or propulsive force). The pitch of the ducted rotor blades is used to maintain a constant X-force and hence can effectively cause the tip-path-plane to tilt over the entire approach velocity range-even at low approach airspeeds. The effect these constant force controllers have on the constant inflow curves is shown for constant drag and constant propulsive force in figures 22 and 23 respectively.

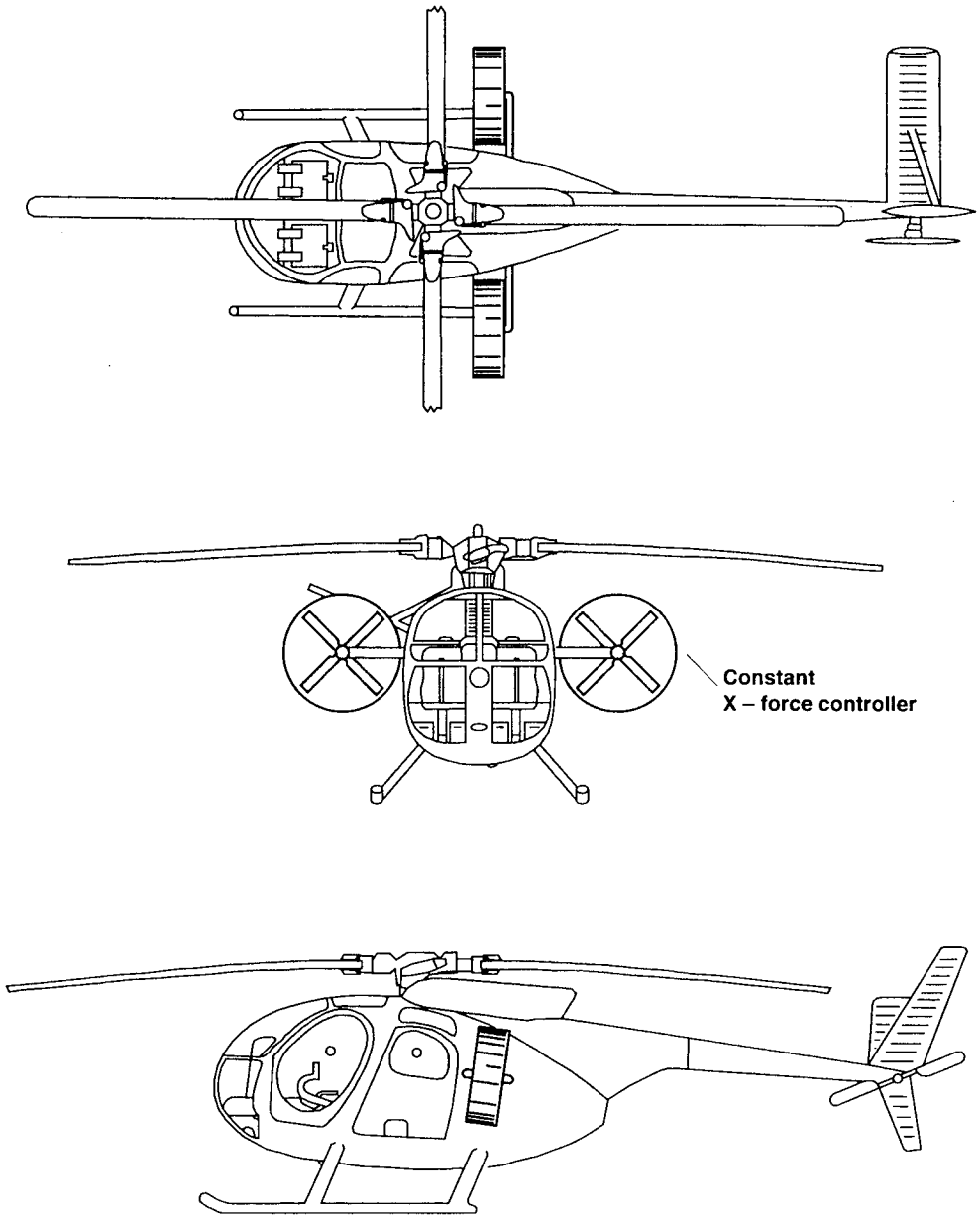

Figure 21. A sketch of a possible constant X-force controller.

The constant drag case, figure 22, acts similarly to the speed brake shown in figure 18. For a $\frac{F_x}{W} = 0.1$, the constant inflow curves are dramatically shifted to higher sink rates at every airspeed. The constant effective drag produced by these auxiliary thrust devices tilts the tip-path-plane of the main rotor more forward (α_{TPP} is more negative) increasing the negative inflow of the main rotor. With the constant drag device deployed at the 70 knot approach airspeed under a 550 ft/minute rate of sink, near zero inflow is avoided therefore reducing the likelihood of a strong BVI noise. At lesser sink rates at this same airspeed, inflow becomes even more negative further decreasing the likelihood of strong BVI noise. At increasing sink rates, inflow approaches zero and strong BVI is again likely.

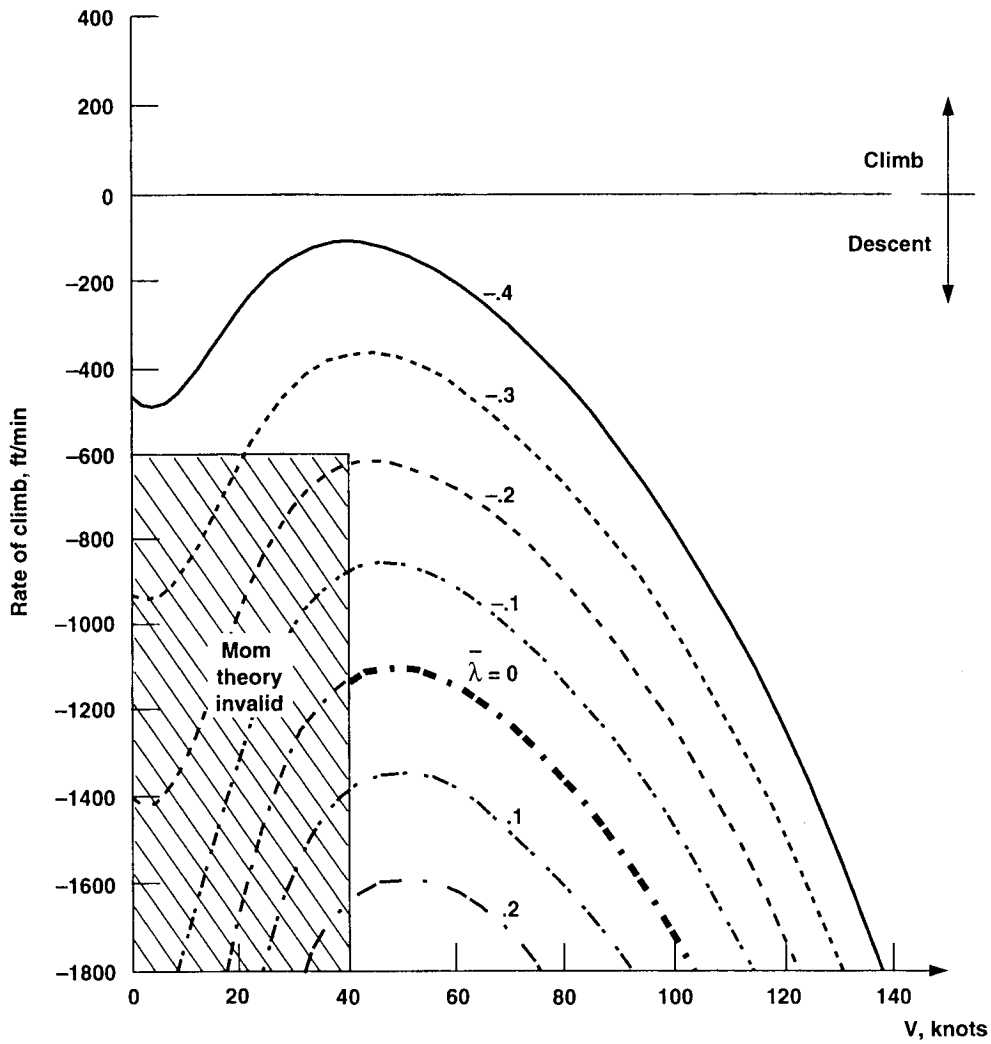

Figure 22. Rate of climb versus forward velocity for several values of constant inflow with constant drag force device deployed (F_x = 0.1).

The effects of a constant propulsive force of $\frac{F_x}{W} = -0.1$ is shown in figure 23. The thrust causes the tip-path-plane to tilt rearward and increases the inflow through the disk in the direction of the thrust vector. In this positive inflow case, the shed vortices pass above the rotor's tip path plane. The auxiliary thrust devices have now placed the helicopter in an autogyro-like mode. At the 70 knots, 550 ft/minute rate of sink, the inflow is now positive, thus reducing the likelihood of BVI noise. Now lower rates of sink reverse this trend and cause near zero inflow conditions to be approached.

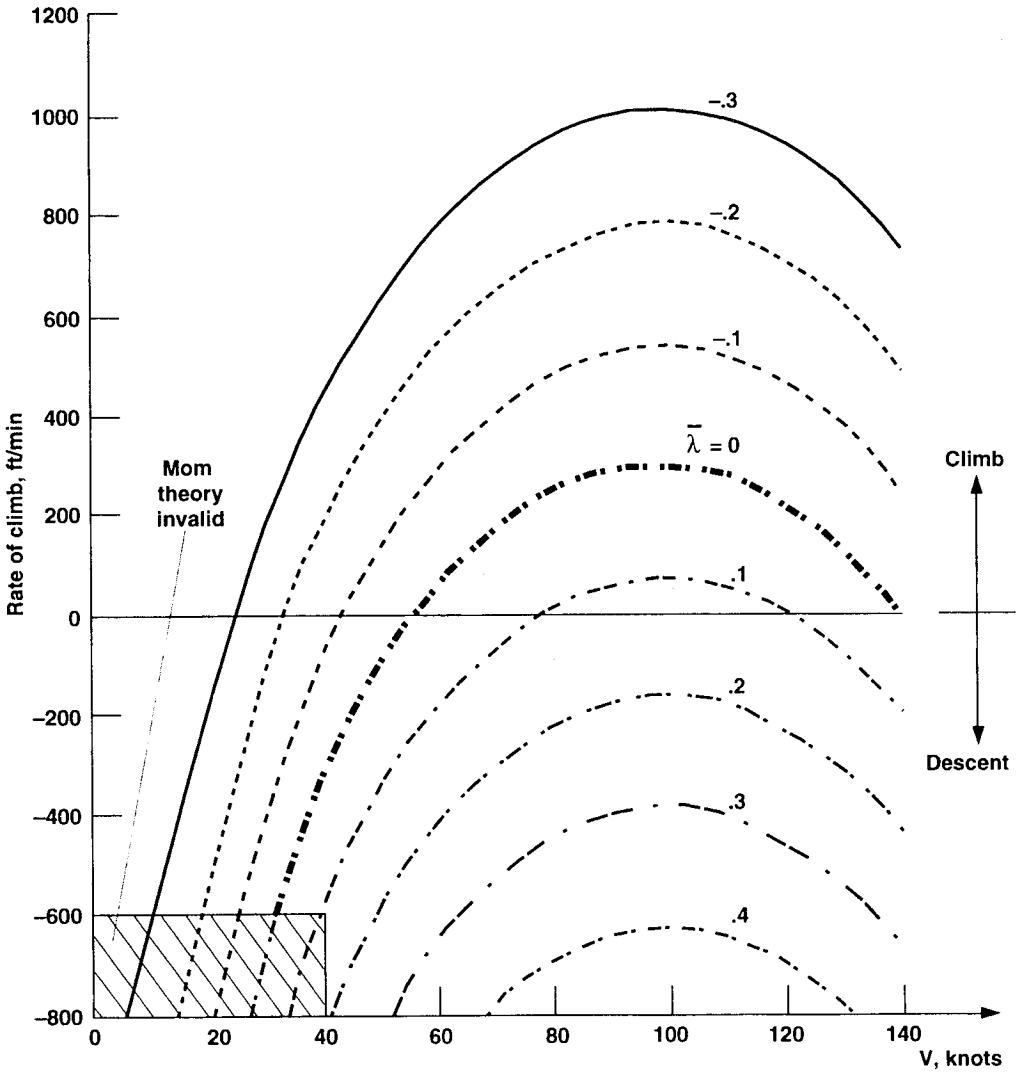

Figure 23. Rate of climb versus forward velocity for several values of constant inflow with a constant propulsive force device deployed ($F_X = -0.1$).

Some Dynamic Performance Observations

An auxiliary X-force controller to minimize BVI noise has been shown to be an effective method of reducing the likelihood of strong BVI noise. This simple analysis has conceptually explored the effectiveness of a few of these X-force producing devices using a quasi-static analysis, where acceleration perpendicular to the flight path has been neglected and acceleration parallel to the flight path has been considered as a parametric variable. In essence, the steady-state longitudinal force equilibrium equations have been solved.

Much of an approach to a conventional landing is performed in this manner. The pilot tries to maintain a constant airspeed and sink-rate until he begins to approach his landing site. At that point, the helicopter is decelerated to reduce airspeed and is flared to arrest the rate of sink. Both of these actions tend to increase BVI. The acceleration perpendicular to the flight path in a flare effectively increases thrust and hence the strength of the tip vortices. Decelerations along the flight path tilt the tip-path-plane further aft (more positive α_{TPP}) and increases the positive inflow through the rotor disk. If the inflow in the approach condition is negative without deceleration, the positive change in inflow due to deceleration can make the net inflow go to zero, resulting in the likelihood of strong BVI. Fortunately, the BVI is confined to the terminal area during deceleration and is probably tolerable.

Using a propulsive force in the "X" direction during approach can avoid strong BVI during the flare and deceleration. Since the inflow in this landing condition is already positive, deceleration only tilts the tip-path-plane further aft further increasing the positive inflow. This moves the shed tip vortices further away from the blades and reduces even further the likelihood of strong BVI.

Conclusions

Simple analytical modeling of the longitudinal trim equations and rotor inflow for a single rotor helicopter have been developed to generally describe the conditions under which BVI is likely during approach to a landing. The model is quasi-static, treating acceleration parallel to the flight path as a parametric variable. This first order modeling has shown that:

- Vehicle drag, increases in climb angle, and acceleration all decrease the rotor's tip-path-plane angle and thus increase the negative inflow through the rotor.
- Increases in descent angle and deceleration increase the rotor's tip-path-plane angle and thus increase the positive inflow through the rotor.
- In steady-state flight during a landing approach, the inflow to the rotor can approach zero. During these conditions, strong BVI is likely. The region where this occurs can be described by a partially bounded region in rate-of-sink versus forward velocity space.

In addition, a new X-force control has been introduced to alter the conditions under which strong BVI is likely. It has been shown that:

- The effect of both a positive and negative X-force control can be used to minimize the likelihood of BVI noise radiation.
- Drag-like devices and constant X-force devices have been conceptually suggested that can produce the required X-forces. These novel concepts need further engineering study, experimentation, and refinement to ensure that low noise BVI conditions can be attained without incurring too much operational complexity or mission performance penalties.

References

1. Cox, C. R.: Subcommittee Chairman's Report to Membership on Aerodynamic Sources of Rotor Noise. Reprint No. 625, 28th Annual Forum, American Helicopter Soc., Inc., May 1972.
2. George, A. R.: Helicopter Noise: State-of-the-Art. Journal of Aircraft, vol. 15, no. 11, 1978, pp. 707–715.
3. White, Richard P., Jr.: The Status of Rotor Noise Technology. Journal of American Helicopter Soc., vol. 25, no. 1, Jan. 1980, pp. 22–29.
4. Schmitz, F. H.; and Yu, Y. H.: Helicopter Impulsive Noise: Theoretical and Experimental Status. Journal of Sound and Vibration, vol. 109, no. 3, Sept. 22, 1986, pp. 361–422.
5. JanakiRam, R. D.: Aeroacoustics of Rotorcraft. AGARD Report 781, 1990.
6. Lowson, M. V.: Progress Towards Quieter Civil Helicopters. Aeronautical Journal, pp. 209–223, June 1992.

7. Tangler, James L.: Schlieren and Noise Studies of Rotors in Forward Flight. 33rd Annual National Forum, American Helicopter Society, Inc., May 1977, pp. 77.33-05-1—77.33-05-12.

8. Halwes, D. R.: Flight Operations to Minimize Noise. Presented at the American Helicopter Society–AIAA–University of Texas at Arlington Joint Symposium on Environmental Effects of VTOL Designs, Arlington, Texas, Nov. 16–18, 1970, and Vertiflite, Feb. 1971.

9. Helicopter Association International (HAI) Fly Neighborly Committee. Fly Neighborly Guide, HAI, Feb. 1992.

10. Chen, R. T. H.; Hindson, W. S.; and Mueller, A. W.: Acoustic Flight Tests of Rotorcraft Noise-Abatement Approaches Using Local Differential GPS Guidance. Presented at the American Helicopter Society Specialists Conference on Rotorcraft Aeromechanical Technologies, Fairfield County, Conn., Oct. 11–13, 1995.

11. Boxwell, D. A.; and Schmitz, F. H.: Full-Scale Measurements of Blade-Vortex Interaction Noise. Journal of the American Helicopter Society, vol. 27, no. 4, Oct. 1982, pp. 11–27.

12. Boxwell, D. A.; and Schmitz, F. H.: In-flight Acoustic Comparison of the 540 and K747 Main Rotors for the AH-1G Helicopter. Production Validation Test-Government: Kaman K747 Improved Main Rotor Blade, USAAEFA Project No. 77-38, U.S. Army, Oct. 1979, pp. 65–90.

13. Gallman, J. M.; and Liu, S. R.: Acoustic Characteristics of Advanced Model Rotor Systems. Presented at the 47th Annual Forum of the American Helicopter Society, 1991.

14. Shenoy, K. R.: The Role of Scale Models in the Design of Low BVI Noise. Presented at the 41st Annual Forum of the American Helicopter Society, May 15–17, 1985.

15. Marcolini, M. A.; Martin, R. M.; Lorber, P. F.; and Egolf, T. A.: Predictions of BVI Noise Patterns and Correlations with Wake Interaction Locations. Presented at the 48th Annual Forum of the American Helicopter Society, Washington, D.C., June 3–5, 1992.

16. Boxwell, D. A.; Schmitz, F. H.; Splettstoesser, W. R.; and Schultz, K. J.: Helicopter Model Rotor-Blade Vortex Interaction Impulsive Noise: Scalability and Parametric Variations. Journal of American Helicopter Society, vol. 32, no. 1, Jan. 1987, pp. 3–12.

REPORT DOCUMENTATION PAGE

Form Approved
OMB No. 0704-0188

1. AGENCY USE ONLY *(Leave blank)*	2. REPORT DATE	3. REPORT TYPE AND DATES COVERED
	September 1995	Technical Memorandum

4. TITLE AND SUBTITLE

Reduction of Blade-Vortex Interaction (BVI) Noise through X-Force Control

5. FUNDING NUMBERS

505-59-36

6. AUTHOR(S)

Fredric H. Schmitz

7. PERFORMING ORGANIZATION NAME(S) AND ADDRESS(ES)

Ames Research Center
Moffett Field, CA 94035-1000

8. PERFORMING ORGANIZATION REPORT NUMBER

A-950104

9. SPONSORING/MONITORING AGENCY NAME(S) AND ADDRESS(ES)

National Aeronautics and Space Administration
Washington, DC 20546-0001

10. SPONSORING/MONITORING AGENCY REPORT NUMBER

NASA TM-110371

11. SUPPLEMENTARY NOTES

Point of Contact: Fredric H. Schmitz, Ames Research Center, MS 258-7, Moffett Field, CA 94035-1000
(415) 604-4080

12a. DISTRIBUTION/AVAILABILITY STATEMENT

Unclassified — Unlimited
Subject Category 05

12b. DISTRIBUTION CODE

13. ABSTRACT ***(Maximum 200 words)***

Momentum theory and the longitudinal force balance equations of a single rotor helicopter are used to develop simple expressions to describe tip-path-plane tilt and uniform inflow to the rotor. The uniform inflow is adjusted to represent the inflow at certain azimuthal locations where strong Blade-Vortex Interaction (BVI) is likely to occur. This theoretical model is then used to describe the flight conditions where BVI is likely to occur and to explore those flight variables that can be used to minimize BVI noise radiation. A new X-force control is introduced to help minimize BVI noise. Several methods of generating the X-force are presented that can be used to alter the inflow to the rotor and thus increase the likelihood of avoiding BVI during approaches to a landing.

14. SUBJECT TERMS	15. NUMBER OF PAGES
Blade-vortex interaction noise, Rotorcraft, Longitudinal trim, Helicopters, Drag devices	30
	16. PRICE CODE: A03

17. SECURITY CLASSIFICATION OF REPORT	18. SECURITY CLASSIFICATION OF THIS PAGE	19. SECURITY CLASSIFICATION OF ABSTRACT	20. LIMITATION OF ABSTRACT
Unclassified	Unclassified		